



Drops on soft solids: free energy and double transition of contact angles

L. A. Lubbers¹, J. H. Weijs^{1,†}, L. Botto², S. Das³, B. Andreotti⁴ and J. H. Snoeijer^{1,5}

¹Physics of Fluids Group, Faculty of Science and Technology, Mesa+ Institute, University of Twente, 7500 AE Enschede, The Netherlands

²School of Engineering and Materials Science, Queen Mary University of London, London E1 4NS, UK

³Department of Mechanical Engineering, University of Maryland, College Park, MD 20742, USA

⁴Physique et Mécanique des Milieux Hétérogènes, UMR 7636 ESPCI-CNRS, Univ. Paris-Diderot, 10 rue Vauquelin, 75005, Paris, France

⁵Department of Applied Physics, Eindhoven University of Technology, PO Box 513, 5600 MB Eindhoven, The Netherlands

(Received 23 December 2013; revised 20 February 2014; accepted 17 March 2014)

The equilibrium shape of liquid drops on elastic substrates is determined by minimizing elastic and capillary free energies, focusing on thick incompressible substrates. The problem is governed by three length scales: the size of the drop R , the molecular size a and the ratio of surface tension to elastic modulus γ/E . We show that the contact angles undergo two transitions upon changing the substrate from rigid to soft. The microscopic wetting angles deviate from Young's law when $\gamma/(Ea) \gg 1$, while the apparent macroscopic angle only changes in the very soft limit $\gamma/(ER) \gg 1$. The elastic deformations are worked out for the simplifying case where the solid surface energy is assumed to be constant. The total free energy turns out to be lower on softer substrates, consistent with recent experiments.

Key words: capillary flows, contact lines, drops

1. Introduction

A liquid drop can deform a soft elastic substrate due to capillary forces (Lester 1961; Rusanov 1975, 1978; Shanahan 1987; de Gennes, Brochard-Wyart & Quere 2004; Pericet-Camara *et al.* 2008*a*). Elastic deformations take place over a length of the order of the elastocapillary length γ/E , where γ is the liquid surface tension

[†] Email address for correspondence: j.h.weijs@gmail.com

and E is the solid Young's modulus. Recent experiments have considered liquids on very soft elastomers with γ/E of the order of 1–100 μm and have reported many interesting features, such as the geometry near the contact line (Pericet-Camara, Bonaccorso & Graf 2008*b*; Jerison *et al.* 2011; Style *et al.* 2013*a*), compression of the solid (Marchand *et al.* 2012*a*), evaporation and spreading dynamics (Carre, Gastel & Shanahan 1996; Li *et al.* 2007; Pericet-Camara *et al.* 2008*b*; Sokuler *et al.* 2010) and migration of droplets on substrates with a stiffness gradient (Style *et al.* 2013*b*).

While the contact angle of a drop on a rigid homogeneous substrate is governed by Young's law, the contact-angle selection for a drop on a soft deformable substrate is still debated. One of the earliest theoretical approaches consisted of treating the elastic energy stored below the contact line as an effective line tension (Shanahan 1987; White 2003; Style & Dufresne 2012). This predicts an increase of the apparent macroscopic contact angle on soft surfaces, which has been contradicted by recent experiments (Style *et al.* 2013*a*). The line-tension approach did not include the surface energy of the solid, which turns out to be a crucial factor for the shaping of soft solids. Such surface effects were introduced by Jerison *et al.* (2011) and Limat (2012) in a purely macroscopic theory based on the balance of forces exerted 'on' the contact line. In this framework, the microscopic contact angles always obey Neumann's law, regardless of E , as if the substrate at the contact line was a liquid. The same work reveals that there exists a transition for the apparent macroscopic contact angle, controlled by the dimensionless parameter $\gamma/(ER)$, where R is the drop size. By contrast, a microscopic description based on van der Waals interactions (Marchand *et al.* 2012*b*) suggests that Young's law for the microscopic contact angle is recovered for $\gamma/(Ea) \ll 1$, where a is the characteristic length of molecular interactions. The formation of a solid cusp below the contact line arises for $\gamma/(Ea) \gg 1$, and the corresponding contact angles generically differ from Neumann's law, even for very soft substrates.

The controversy on the selection of contact angles on soft substrates underlines the difficulty of defining a force balance near the contact line (Marchand *et al.* 2011). This has two distinct reasons: on the one hand, the difference between macroscopic and microscopic descriptions of capillarity, and on the other hand, the difference between surface stress Υ (force per unit length), which is manifested in the superficial layers of a solid, and surface free energy γ (energy per unit area). The latter is due to the coupling of elastic strain and surface free energy, an effect that is absent for liquid–liquid interfaces. Surface stress and surface energy are related by a thermodynamic law known as the Shuttleworth equation, $\Upsilon = \gamma + (d\gamma/d\epsilon_{\parallel})$, where ϵ_{\parallel} is the elastic strain parallel to the interface (Shuttleworth 1950). The strain dependence $d\gamma/d\epsilon_{\parallel}$ is directly responsible for tangential elastic stress transmitted below the contact line (Das *et al.* 2011; Marchand *et al.* 2012*a*; Weijs, Andreotti & Snoeijer 2013), usually ignored in elasto-capillary modelling.

In this paper we revisit the contact-angle selection from a thermodynamic perspective, using variational calculus, i.e. without relying on a mechanical view in terms of a force balance. The challenge is to derive the contact angles directly by minimizing the capillary and elastic free energies. An important question then is whether microscopic and macroscopic descriptions of capillarity will give consistent results. To make progress, we restrict ourselves to the case where the Shuttleworth effect is absent, i.e. $d\gamma/d\epsilon_{\parallel} = 0$, for which it was previously shown that the tangential elastic stress vanishes (Weijs *et al.* 2013). Combined with an incompressible thick substrate (Poisson ratio $\nu = 1/2$), this implies no in-plane displacements, making the problem amenable for detailed variational analysis.

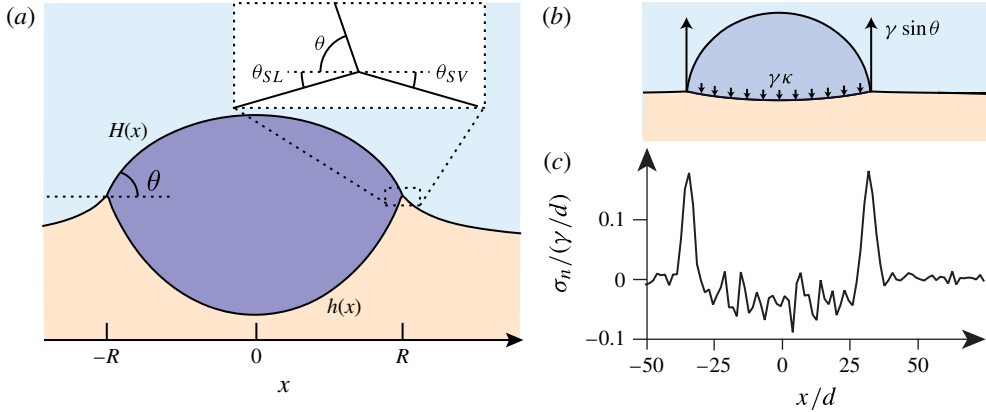


FIGURE 1. (a) The liquid and solid surface shapes are described by $H(x)$ and $h(x)$ respectively. The contact line geometry is characterized by the angles θ , θ_{SV} and θ_{SL} (see inset). (b,c) Normal component of capillary stress exerted on the solid. (b) Macroscopic view given by (2.14). A force per unit length is pulling on the solid at the contact-line positions while a Laplace pressure is applied below the drop. (c) Microscopic view of the normal stress σ_n below a Lennard-Jones nanodroplet in a Molecular Dynamics simulation (adapted from Weijs *et al.* (2013)). The force near the contact lines is spread over a finite width a of a few molecular sizes (units in terms of molecular size d). At the centre of the drop one recognizes the slightly negative capillary stress.

The key questions resolved here are how the contact angles and the elasto-capillary free energies evolve upon changing the substrate from perfectly rigid (no deformation) to extremely soft (no elasticity). We predict the angles θ , θ_{SV} and θ_{SL} , as defined in figure 1(a), as a function of the ‘softness parameters’ $\gamma/(Ea)$ and $\gamma/(ER)$. We show that both parameters govern a transition from Young’s law to Neumann’s law, but apply to different features of the angles in figure 1. This reveals the connection between previously proposed results in a single framework. Finally, the full shapes of the drops and the surface deflections are worked out for a case where the solid surface energies $\gamma_{SV} = \gamma_{SL}$. We find that the free energy is lower on softer substrates, and relate this to experiments on drop motion on substrates exhibiting a stiffness gradient (Style *et al.* 2013b).

2. Equilibrium conditions from variational analysis

2.1. Macroscopic theory of capillarity

2.1.1. A single contact line

Considering a semi-infinite incompressible solid ($\nu = 1/2$) in a two-dimensional system, the elastic free energy per unit length can be expressed as a surface integral,

$$\mathcal{F}_{el} = \frac{E}{2} \int_{-\infty}^{\infty} \frac{dq}{2\pi} \widehat{Q}(q) \left[\hat{h}(q)\hat{h}(-q) + \hat{u}(q)\hat{u}(-q) \right], \quad (2.1)$$

where $\hat{h}(q)$ and $\hat{u}(q)$ are Fourier transforms of the normal and tangential displacements, $h(x)$ and $u(x)$, at the interface (Long, Ajdari & Leibler 1996). The Green’s function reads $\widehat{Q}(q) = 2|q|/3$ in the incompressible limit.

Before analysing a two-dimensional drop (figure 1), we consider the simpler case of a single contact line located at $x=R$. The liquid–vapour interface is described by $H(x)$, while $h(x)$ is the profile of the solid surface. When useful, we will use the indexed notation h_{SL} or h_{SV} to distinguish whether the solid is wet or dry, with surface free energies γ_{SL} and γ_{SV} . The total surface free energy in this case is

$$\mathcal{F}_c = \gamma \int_{-\infty}^R dx (1 + H'^2)^{1/2} + \gamma_{SL} \int_{-\infty}^R dx (1 + h_{SL}'^2)^{1/2} + \gamma_{SV} \int_R^{\infty} dx (1 + h_{SV}'^2)^{1/2}, \quad (2.2)$$

where ∞ refers to a very large (finite) distance far away from the contact line. We anticipate a slope discontinuity $h_{SV}' \neq h_{SL}'$ at $x=R$. The condition that H , h_{SL} and h_{SV} take the same value at the contact line can be enforced by introducing two Lagrange multipliers, λ_{SL} and λ_{SV} , into the energy functional,

$$\mathcal{F}_{tot} = \mathcal{F}_{el} + \mathcal{F}_c + \lambda_{SL} [H(R) - h_{SL}(R)] + \lambda_{SV} [H(R) - h_{SV}(R)], \quad (2.3)$$

where the Lagrange multipliers can be interpreted as reaction forces (per unit length). Minimization must be performed with respect to $H(x)$, $h(x)$ and the contact line position R . As explained in the introduction, the tangential displacements $u(x)$ vanish when the surface free energies are assumed to be constant, i.e. independent of the elastic strain.

First, we consider the variation $\delta H(x)$, which gives

$$\delta \mathcal{F}_{tot} = \delta H(R) \left[\lambda_{SL} + \lambda_{SV} + \frac{\gamma H'}{(1 + H'^2)^{1/2}} \right] + \int_{-\infty}^R dx \delta H(x) [-\gamma \kappa]. \quad (2.4)$$

The boundary term $\delta H(R)$ originates from the constraints on the contact-line position and from the integration by parts of the capillary term \mathcal{F}_c with respect to $\delta H'$ and gives $\lambda_{SL} + \lambda_{SV} = \gamma \sin \theta$. The second term on the right-hand side involves the curvature $\kappa = H''/(1 + H'^2)^{3/2}$, which is zero for a single contact line.

Second, we consider the variation $\delta h(x)$, which gives

$$\begin{aligned} \delta \mathcal{F}_{tot} = & \delta h_{SL}(R) \left[-\lambda_{SL} + \frac{\gamma_{SL} h_{SL}'}{(1 + h_{SL}'^2)^{1/2}} \right] + \delta h_{SV}(R) \left[-\lambda_{SV} - \frac{\gamma_{SV} h_{SV}'}{(1 + h_{SV}'^2)^{1/2}} \right] \\ & + \int_{-\infty}^R dx \delta h_{SL}(x) [-\gamma_{SL} \kappa_{SL}] + \int_R^{\infty} dx \delta h_{SV}(x) [-\gamma_{SV} \kappa_{SV}] \\ & + \int_{-\infty}^{\infty} dx \delta h(x) \left[E \int_{-\infty}^{\infty} \frac{dq}{2\pi} \widehat{Q}_n(q) \hat{h}(q) e^{iqx} \right], \end{aligned} \quad (2.5)$$

where the first four terms in brackets are analogous to those in (2.4), but they now express vertical forces acting on a corner of solid. The last term represents the inverse Fourier transform of the variation of \mathcal{F}_{el} , and involves the elastic normal stress

$$\sigma_n(x) \equiv E \int_{-\infty}^{\infty} \frac{dq}{2\pi} \widehat{Q}_n(q) \hat{h}(q) e^{iqx}. \quad (2.6)$$

When σ_n contains a Dirac δ -function at $x=R$, this elastic stress could contribute to the boundary condition at $x=R$, but within the macroscopic framework this can be excluded on mathematical grounds. As $\widehat{Q} \sim |q|$, a δ -function contribution

would require a (weakly) singular displacement, $h \sim \log|x - R|$, and hence a (weakly) diverging elastic free energy. The equilibrium condition at the contact line is therefore determined by the surface energies only (Jerison *et al.* 2011; Limat 2012), implying a weaker singularity in the form of a discontinuity in h' . One can show that this implies a weakly diverging stress, $\sigma_n \sim \log|x - R|$, but an integrable free energy. Given this singularity, the physics may be significantly different when microscopic effects are included.

Following for now the macroscopic derivation, the variations at the contact line, $\delta h(R)$, determine the Lagrange multipliers, $\lambda_{SL} = \gamma_{SL} \sin \theta_{SL}$ and $\lambda_{SV} = \gamma_{SV} \sin \theta_{SV}$. Combined with the boundary condition resulting from (2.4), these expressions give

$$\gamma \sin \theta = \gamma_{SL} \sin \theta_{SL} + \gamma_{SV} \sin \theta_{SV}, \quad (2.7)$$

which can be recognized as the vertical component of the Neumann condition. This condition is analogous to that describing a liquid lens floating on another liquid, since the elastic energy does not give a contribution at the contact line. The mechanical equilibrium away from the contact line can be obtained by combining the integrals in (2.5), giving

$$\sigma_n(x) = \gamma_{SL} \kappa_{SL} \Theta(R - x) + \gamma_{SV} \kappa_{SV} \Theta(x - R) \equiv \gamma_s(x) \frac{h''}{(1 + h^2)^{3/2}}, \quad (2.8)$$

where $\Theta(x)$ is the Heaviside step function and $\gamma_s(x)$ is the solid surface tension on the respective domain. This expression is not defined at $x = R$, where instead it is replaced by a boundary condition (2.7). For $x \neq R$, the stress σ_n balances the Laplace pressure due to the curvature κ_{SL} (κ_{SV}) of the wet (dry) solid interface.

We now consider variations δR of the contact-line position. This variation has contributions from the integration limits in \mathcal{F}_c , from the contact-line constraints (terms involving $\lambda_{SL} + \lambda_{SV}$), but once again not from the elastic energy contribution \mathcal{F}_{el} . The total variation (to be evaluated at $x = R$) gives

$$\begin{aligned} \delta \mathcal{F}_{tot} &= \delta R \{ \gamma (1 + H^2)^{1/2} + \gamma_{SL} (1 + h_{SL}^2)^{1/2} - \gamma_{SV} (1 + h_{SV}^2)^{1/2} \\ &\quad + (\lambda_{SV} + \lambda_{SL}) H' - \lambda_{SL} h'_{SL} - \lambda_{SV} h'_{SV} \} \\ &= \delta R \left\{ \frac{\gamma}{(1 + H^2)^{1/2}} + \frac{\gamma_{SL}}{(1 + h_{SL}^2)^{1/2}} - \frac{\gamma_{SV}}{(1 + h_{SV}^2)^{1/2}} \right\}, \end{aligned} \quad (2.9)$$

where we inserted the values for λ_{SL} and λ_{SV} obtained previously. In terms of the angles indicated in figure 1, this expression gives the horizontal Neumann condition,

$$\gamma \cos \theta + \gamma_{SL} \cos \theta_{SL} = \gamma_{SV} \cos \theta_{SV}. \quad (2.10)$$

To summarize, we recover the usual Laplace pressure condition for the liquid interface $H(x)$. The solid interface shape $h(x)$ follows from the balance (2.8) of elastic stress σ_n and solid Laplace pressure. The problem is closed by the vertical and horizontal Neumann conditions (2.7), (2.10), serving as boundary conditions for the angles at the contact line.

2.1.2. A two-dimensional drop

We now consider a two-dimensional drop with contact lines at $x = R$ and $x = -R$. The expression for the free energy is similar to that for a single contact line, except that we have to consider two dry domains, $x > R$ and $x < -R$, and one wet domain, $-R < x < R$. In addition, minimization is carried out at constant drop volume V . This constraint is enforced by adding the Lagrange multiplier term

$$\mathcal{F}_V = P \left[V - \int_{-R}^R dx (H(x) - h(x)) \right] \quad (2.11)$$

to the total energy. Since $H(x) = h(x)$ at $x = \pm R$, the volume constraint does not contribute to the boundary conditions, and we recover (2.7) and (2.10). It does, however, introduce a contribution to the equilibrium equations for $H(x)$ and $h(x)$, namely

$$-\gamma\kappa = P, \quad \sigma_n(x) = -P\Theta(R - |x|) + \gamma_s(x) \frac{h''}{(1 + h'^2)^{3/2}}. \quad (2.12a,b)$$

The first relation requires the liquid interface to have a constant curvature, corresponding to the Laplace pressure $P = \gamma \sin \theta / R$. The second equation shows that P also acts as an external stress on the boundary of the elastic medium below the drop. It is instructive to incorporate the vertical boundary condition (2.7) in the elastic stress, as

$$\sigma_n = \gamma \sin \theta f_n(x) + \left(\frac{\gamma_s(x) h'}{(1 + h'^2)^{1/2}} \right)', \quad (2.13)$$

where $f_n(x)$ is the distribution of normal stress due to the capillary forces,

$$f_n(x) = \delta(x - R) + \delta(x + R) - \frac{1}{R} \Theta(R - |x|). \quad (2.14)$$

This corresponds to the classical mechanical view of two localized forces pulling upwards at the contact line and a Laplace pressure pushing downward below the drop (figure 1b).

2.2. Microscopic theory of capillarity

In the limit of perfectly rigid solids one would expect to recover Young's law. However, the macroscopic theory derived above shows that the wetting angles are given by the Neumann conditions *regardless of the stiffness*, which is clearly unphysical. Also, the elastic stress was found to be singular at the contact line. These artefacts are due to the assumption of localized line forces represented by δ -functions in (2.14). Because the interface is diffuse at the molecular level and due to the finite range of van der Waals interactions, capillary forces are in reality spread out over a finite width a , typically a few nanometres. This is illustrated in figure 1(c), showing the normal stress exerted by a nanodroplet on an elastic substrate as measured in a Molecular Dynamics simulation (Weijs *et al.* 2013).

The finite width of the interface can be taken into account in a truly microscopic description, using a disjoining pressure (White 2003) or density functional theory (Das *et al.* 2011; Marchand *et al.* 2012b). Here, we propose a simplified model which

captures the essence of these microscopic models, but still allows for a numerical solution with realistic separation of the microscopic scale ($a \sim \text{nm}$) and macroscopic scale ($R \sim \text{mm}$). The approach consists of retaining the boundary condition (2.10), but representing the line forces in (2.14) by a function g of finite width

$$f_n(x) = \frac{1}{a}g\left(\frac{x-R}{a}\right) + \frac{1}{a}g\left(\frac{x+R}{a}\right) - \frac{1}{R}\Theta(R-|x|). \quad (2.15)$$

In our numerical solutions, g is chosen as a normalized Gaussian, but other choices give similar results. With this approach, the contact angles display two distinct transitions which are governed by the parameters $\gamma/(Ea)$ and $\gamma/(ER)$.

2.3. Dimensionless equations and solution strategy

It is challenging to solve for $h(x)$ from (2.13) due to the integral nature of σ_n , the discontinuity in $\gamma_s(x)$ and the presence of nonlinear terms. We simplify the problem by considering the case $\gamma_{SV} = \gamma_{SL} = \gamma_s$ and assume $h^2 \ll 1$ to linearize the last term in (2.13); the latter condition is enforced by choosing moderate values of γ/γ_s . We then solve the resulting equation by Fourier transform. In the following we rescale all lengths by R and the pressure by γ/R . The macroscopic model depends on two dimensionless parameters, $\gamma/(ER)$ and γ/γ_s . The microscopic model has an additional parameter, $\tilde{a} = a/R$, or equivalently $\gamma/(Ea)$. Solving for the profile in Fourier space, $\hat{h}(q)$, (2.13) gives

$$\hat{h}(q) = \frac{\gamma}{ER} \sin \theta \left\{ \frac{\hat{f}_n(q, \tilde{a}) \hat{\mathcal{K}}(q)}{1 + \frac{\gamma}{ER} \frac{\gamma_s}{\gamma} q^2 \hat{\mathcal{K}}(q)} \right\}, \quad (2.16)$$

where

$$\hat{f}_n(q, \tilde{a}) = 2 \left(e^{-1/2(\tilde{a}q)^2} \cos q - \frac{\sin q}{q} \right) \quad \text{and} \quad \hat{\mathcal{K}}(q) \equiv \hat{Q}^{-1}(q) = \frac{3}{2|q|}. \quad (2.17a,b)$$

The macroscopic theory corresponds to $\tilde{a} = 0$. Numerical solutions for $h(x)$ that satisfy (2.10) are obtained iteratively, by adjusting θ . Typical results are shown in figure 2. The assumption $\gamma_{SV} = \gamma_{SL}$ makes the contact line left–right symmetric in the rigid limit. For $\gamma_{SV} \neq \gamma_{SL}$ this symmetry is broken, but the results will be qualitatively the same.

3. Numerical results

3.1. Microscopic and macroscopic contact angles: two transitions

We now describe how the wetting angles depend on the stiffness of the substrate. It is important to distinguish between the microscopic wetting angles, θ_s , θ_{SL} and θ_{SV} (figure 3), and the macroscopic angle, θ (figure 1a). The former angles reveal the microscopic geometry of the contact-line region, while the latter is the apparent angle of the spherical cap with respect to the undeformed substrate. The results presented in figure 3 are obtained for $\gamma/\gamma_s = 0.1$, $\tilde{a} = 10^{-5}$ and Young's angle $\theta_Y = 90^\circ$ (since $\gamma_{SV} = \gamma_{SL}$).

Our key finding is that the wetting angles undergo two transitions on changing the softness parameter: (i) the *microscopic* angles evolve continuously from Young's law (rigid limit) to Neumann's law (soft limit), controlled by the parameter $\gamma/(Ea)$;

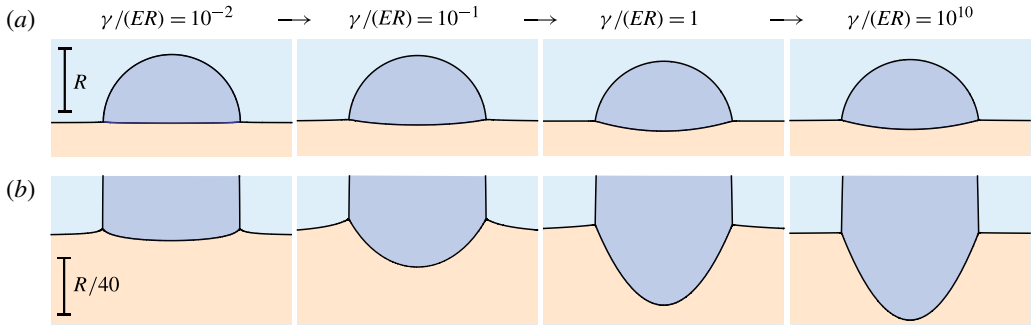


FIGURE 2. Simulated shapes of the drop (dark blue) and of the solid substrate (light orange) for different values of $\gamma/(ER)$, $\gamma/\gamma_s = 0.3$ and $\tilde{a} = 0$. (a) As the solid becomes softer (increasing $\gamma/(ER)$) the drop sinks increasingly deeper into the substrate. (b) Zoom near the contact-line region, with the vertical scale stretched 40 times. The elevation at the contact line initially increases for increasing softness, but on further increasing the softness the elevation subsequently decreases.

(ii) the *macroscopic* apparent contact angle θ evolves continuously from Young’s law (rigid limit) to Neumann’s law (soft limit), controlled by the parameter $\gamma/(ER)$. As discussed in more detail below, these soft and rigid limits are known analytically, while for the transition regions described in figure 3 we rely on numerical solution of (2.16) and (2.10).

For $\gamma/(Ea) \ll 1$, in the perfectly rigid limit, the microscopic solid angle is unchanged, i.e. $\theta_s = 180^\circ$, while the liquid angle $\theta = \theta_\gamma$ is equal to Young’s angle. At the first transition, $\gamma/(Ea) \sim 1$, the solid angle changes and the geometry evolves towards a Neumann cusp. This transition is quantified in the plot in figure 3, where the solid line on the left measures the solid deflection $\pi - \theta_s = \theta_{sv} + \theta_{sl}$ for different values of the softness. In this regime the macroscopic angle $\theta = \theta_\gamma = 90^\circ$ does not change, and hence the geometry is fully characterized by the single angle θ_s . The Neumann cusp, unlike what is predicted by macroscopic theory, is not present for all values of the stiffness and is only recovered for $\gamma/(Ea) \gg 1$.

The second transition does involve the apparent contact angle θ . As long as $\gamma/(ER) \ll 1$, this angle is unaffected by elastic deformations, as these deformations are localized only in a narrow zone near the contact line. The macroscopic angle changes only when the scale of the deformation γ/E becomes comparable to the drop size R , i.e. when $\gamma/(ER) \sim 1$. In the very soft limit the angle saturates, reaching the value expected for a liquid lens. As is visible in the sketches in figure 3, the solid–vapour angle $\theta_{sv} = 0$ in this limit, consistent with previous predictions (Limat 2012; Style & Dufresne 2012). Microscopically, the geometry of the contact angles is completely specified by the amount of rotation of the Neumann angles, as is indicated by the angle ϵ (figure 3a). The transition is quantified by the solid line in the plot of figure 3(b), where we observe how the rotation angle ϵ evolves from the limits corresponding to Young and to that of Neumann. Indeed, the crossover is observed around $\gamma/(ER) \sim 1$.

For completeness, we also carried out the macroscopic analysis for three-dimensional axisymmetric drops. The analysis is analogous to that in the two-dimensional case, except that we use the Hankel transform (Style & Dufresne 2012). As we here self-consistently determine the value of the angle θ , we are

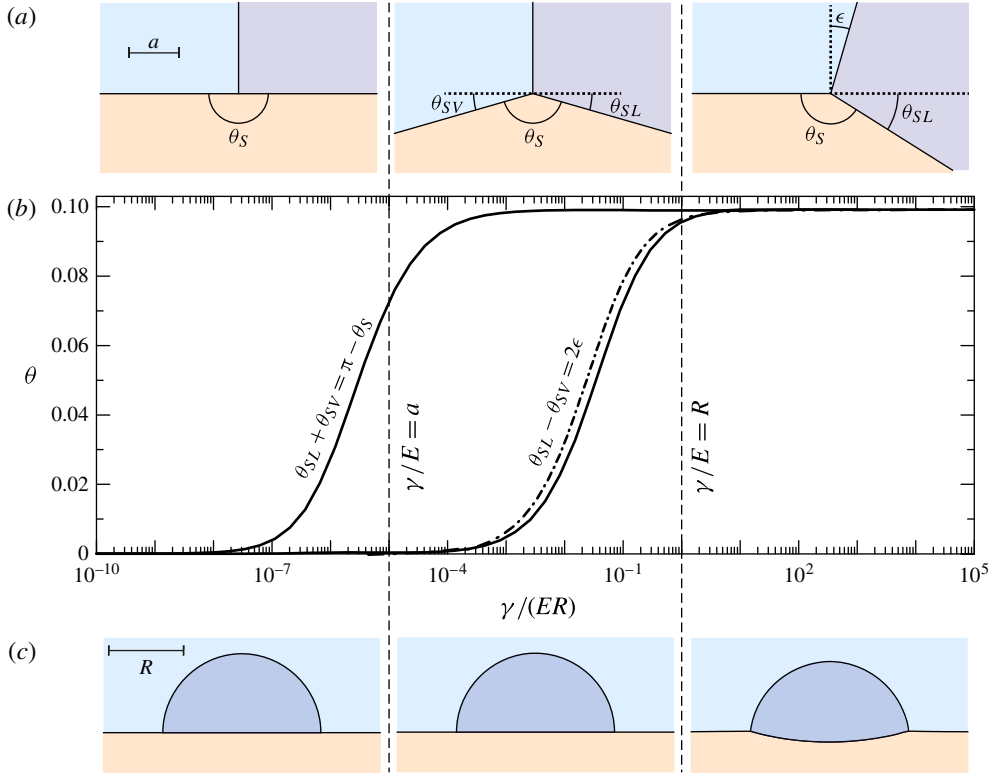


FIGURE 3. Double transition of contact-line angles, for 2D drops (solid curve) and 3D drops (dashed curve). The stiffness is varied by the softness parameter $\gamma/(ER)$, at fixed $\gamma/\gamma_s = 0.1$ and $\tilde{a} = 10^{-5}$. The left-hand curve gives the deviation of the solid angle, $\pi - \theta_S$, showing the onset of the cusp. The right-hand curves give the cusp rotation angle ϵ , defined from the microscopic wetting angles (panel (a), scale a). Panel (c) shows the corresponding macroscopic drop shapes. This shows that (i) the microscopic geometry of the contact line develops a Neumann-like cusp when γ/E is much larger than the microscopic scale a and (ii) the macroscopic angle of the drop is altered only when γ/E reaches the size of the drop R .

for the first time able to assess the validity of the ‘elastic line tension’ argument (White 2003; Style & Dufresne 2012). The result for the deflection angle ϵ is shown as the dash-dotted curve in figure 3, from which it is apparent that this angle is almost indistinguishable from that obtained in the two-dimensional case. The trend for θ , decreasing when reducing the stiffness, is *opposite* to that predicted by considering a positive line tension, but is in agreement with recent experiments (figure 3a of Style *et al.* (2013a)).

3.2. Elevation of the contact line and total energy versus softness

While varying $\gamma/(ER)$ we observe that the elevation of the contact line for the macroscopic model ($\tilde{a} = 0$) evolves non-monotonically (cf. figure 2). This is quantified in figure 4, showing the contact-line elevation $h(x/R = 1)$ as a function of $\gamma/(ER)$. The contact-line elevation $h(1)$ has a maximum for $\gamma/(ER) \sim 0.1$. In the stiff limit ($E \rightarrow \infty$) the solid opposes any stress without deforming while in the soft limit

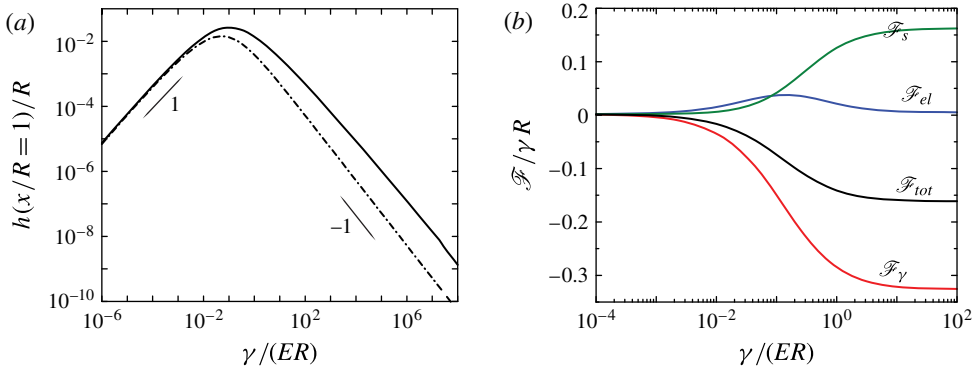


FIGURE 4. (a) Elevation at the contact line as a function of $\gamma/(ER)$ for $\gamma/\gamma_s = 0.1$. The solid curve is the result from 2-D theory and the dash-dotted curve is from 3-D theory. The deformations at the contact line are non-monotonic, as also seen in figure 2. (b) Elastic energy \mathcal{F}_{el} , capillary solid energy \mathcal{F}_s and capillary liquid energy \mathcal{F}_γ as a function of $\gamma/(ER)$ for $\gamma/\gamma_s = 0.5$. The total free energy decreases as the softness increases. The reference energy ($E = 0$) is a drop on a rigid solid.

($E \rightarrow 0$) the geometry of the drop–substrate interface is identical to that of a floating liquid lens. From the numerical results we find that the contact-line height fits closely to

$$h(x/R=1) \sim \left(\frac{\gamma}{ER}\right) \ln(\gamma/ER) \quad \text{and} \quad h(x/R=1) \sim \left(\frac{\gamma}{ER}\right)^{-1} \ln(ER/\gamma), \quad (3.1a,b)$$

for small and large $\gamma/(ER)$, respectively. The rigid limit was previously found by Limat (2012), who showed that for weak deformations the solid surface tension provides a natural regularization of the logarithmic divergence at the contact line. The dash-dotted curve (three-dimensional drop), suggests an $h \sim (\gamma/(ER))^{-1}$ dependence for $\gamma/(ER) \gg 1$.

Another characteristic of the deformation is the central deflection, $h(x/R=0)$. As seen in figure 2, this deflection increases monotonically with the softness, starting from zero (drop on rigid solid) and saturating at the value for a floating lens. The crossover between these limits is again governed by the macroscopic length, and lies around $\gamma/(ER) \sim 0.1$.

Finally, we calculate the elastic energy (\mathcal{F}_{el}), the solid capillary energy (\mathcal{F}_s) and the liquid capillary energy (\mathcal{F}_γ) for a droplet on a substrate of varying stiffness (see figure 4b). In these calculations, the droplet volume is kept constant. This allows for a direct comparison with recent experiments by Style *et al.* (2013b), where droplets were found to move to softer regions on a substrate with a stiffness gradient. Our calculations, which predict a lower total energy $\mathcal{F}_{tot} \equiv \mathcal{F}_{el} + \mathcal{F}_s + \mathcal{F}_\gamma$ for droplets on softer substrates, provide an explanation for this observation. The energies \mathcal{F}_{el} and \mathcal{F}_s actually increase for softer surfaces, but by a smaller amount than the gain in the liquid–vapour energy (\mathcal{F}_γ).

4. Discussion

In this work, we have calculated the shapes of drops on soft substrates by minimization of the elastic and capillary energies. We found that in addition to

the drop size R and the elastocapillary length γ/E , a third length scale is required in order to fully describe the elastocapillary interactions, the molecular scale a . This extra length scale is crucial for the description of the Young to non-Young transition that occurs for sessile droplets on progressively softer substrates. In addition, the regularization is necessary to avoid a singularity of the elastic stress at the contact line. Such a singular tendency implies that, generically, the substrates will be deformed beyond the linear elastic regime – one expects strain hardening and even plasticity (Limat 2012) – which to date has never been taken into account. In addition, the elastic free energy posed in (2.1) is strictly speaking only valid for small slopes of the solid substrate; this is why our numerical results in figure 2 were chosen at moderate γ/γ_s . For larger slopes one, in principle, has to deal with this ‘geometric’ nonlinearity, even if one assumes that the rheology of the elastic solid remains linear. It is not clear *a priori* whether this would lead to an elastic contribution to the Neumann boundary condition for soft solids.

In order to derive the present results, we have left out the second difficulty of the problem, namely the strain dependence of the surface free energies (Shuttleworth effect). Such a strain dependence has been shown to lead to significant tangential elastic stress (Weijs *et al.* 2013). Generically, this induces tangential displacements that are comparable in magnitude to the normal deflection of the substrate, hence changing the energetics of the problem. We emphasize again that this effect is of primary importance for *quantitative* comparison with experiments, the more so since tangential stresses are expected to give an elastic contribution to the contact-angle boundary condition (Marchand *et al.* 2012*b*). Qualitatively, however, the present model does capture two key experimental observations: a softer substrate leads to a decrease of the macroscopic contact angle and to a decrease in the total free energy. The derivation of the contact-angle selection and substrate deformation including all difficulties mentioned above (nonlinearities and Shuttleworth effect) is the next major challenge for the field.

References

- CARRE, A., GASTEL, J. C. & SHANAHAN, M. E. R. 1996 Viscoelastic effects in the spreading of liquids. *Nature* **379** (6564), 432–434.
- DAS, S., MARCHAND, A., ANDREOTTI, B. & SNOEIJER, J. H. 2011 Elastic deformation due to tangential capillary forces. *Phys. Fluids* **23** (7), 072006.
- DE GENNES, P.-G., BROCHARD-WYART, F. & QUERE, D. 2004 *Capillarity and Wetting Phenomena: Drops, Bubbles, Pearls, Waves*. Springer.
- JERISON, E. R., XU, Y., WILEN, L. A. & DUFRESNE, E. R. 2011 Deformation of an elastic substrate by a three-phase contact line. *Phys. Rev. Lett.* **106** (18), 186103.
- LESTER, G. R. 1961 Contact angles of liquids at deformable solid surfaces. *J. Colloid Sci.* **16** (4), 315–326.
- LI, G., GRAF, K., BONACCURSO, E., GOLOVKO, D. S., BEST, A. & BUTT, H.-J. 2007 Evaporation structures of solvent drops evaporating from polymer surfaces: influence of molar mass. *Macromol. Chem. Phys.* **208** (19–20), 2134–2144.
- LIMAT, L. 2012 Straight contact lines on a soft, incompressible solid. *Eur. Phys. J. E* **35** (12), 134.
- LONG, D., AJDARI, A. & LEIBLER, L. 1996 Static and dynamic wetting properties of thin rubber films. *Langmuir* **12** (21), 5221–5230.
- MARCHAND, A., DAS, S., SNOEIJER, J. H. & ANDREOTTI, B. 2012*a* Capillary pressure and contact line force on a soft solid. *Phys. Rev. Lett.* **108**, 094301.
- MARCHAND, A., DAS, S., SNOEIJER, J. H. & ANDREOTTI, B. 2012*b* Contact angles on a soft solid: from Young’s law to Neumann’s law. *Phys. Rev. Lett.* **109** (23), 236101.
- MARCHAND, A., WEIJS, J. H., SNOEIJER, J. H. & ANDREOTTI, B. 2011 Why is surface tension a force parallel to the interface? *Am. J. Phys.* **79** (10), 999–1008.

- PERICET-CAMARA, R., BEST, A., BUTT, H.-J. & BONACCURSO, E. 2008a Effect of capillary pressure and surface tension on the deformation of elastic surfaces by sessile liquid microdrops: an experimental investigation. *Langmuir* **24** (19), 10565–10568.
- PERICET-CAMARA, R., BONACCURSO, E. & GRAF, K. 2008b Microstructuring of polystyrene surfaces with nonsolvent sessile droplets. *ChemPhysChem* **9** (12), 1738–1746.
- RUSANOV, A. I. 1975 Theory of wetting of elastically deformed bodies. I. Deformation with a finite contact-angle. *Colloid J. USSR* **37** (4), 614–622.
- RUSANOV, A. I. 1978 Thermodynamics of deformable solid-surfaces. *J. Colloid Interface Sci.* **63** (2), 330–345.
- SHANAHAN, M. E. R. 1987 The influence of solid micro-deformation on contact-angle equilibrium. *J. Phys. D: Appl. Phys.* **20** (7), 945–950.
- SHUTTLEWORTH, R. 1950 The surface tension of solids. *Proc. Phys. Soc. Lond. A* **63** (365), 444–457.
- SOKULER, M., AUERNHAMMER, G. K., ROTH, M., LIU, C., BONACCURSO, E. & BUTT, H.-J. 2010 The softer the better: fast condensation on soft surfaces. *Langmuir* **26** (3), 1544–1547.
- STYLE, R. W., BOLTYANSKIY, R., CHE, Y., WETTLAUFER, J. S., WILEN, L. A. & DUFRESNE, E. R. 2013a Universal deformation of soft substrates near a contact line and the direct measurement of solid surface stresses. *Phys. Rev. Lett.* **110**, 066103.
- STYLE, R. W., CHE, Y., PARK, S. J., WEON, B. M., JE, J. H., HYLAND, C., GERMAN, G. K., POWER, M. P., WILEN, L. A., WETTLAUFER, J. S. & DUFRESNE, E. R. 2013b Patterning droplets with durotaxis. *Proc. Natl Acad. Sci. USA*.
- STYLE, R. W. & DUFRESNE, E. R. 2012 Static wetting on deformable substrates, from liquids to soft solids. *Soft Matt.* **8** (27), 7177–7184.
- WEIJS, J. H., ANDREOTTI, B. & SNOEIJER, J. H. 2013 Elasto-capillarity at the nanoscale: on the coupling between elasticity and surface energy in soft solids. *Soft Matt.* **9**, 8494–8503.
- WHITE, L. R. 2003 The contact angle on an elastic substrate. 1. The role of disjoining pressure in the surface mechanics. *J. Colloid Interface Sci.* **258** (1), 82–96.